

Transitions in polycrystalline diamond probed by steady state, modulated and transient surface photovoltage spectroscopy

Thomas Dittrich^{1,*}  and Steffen Fengler² 

¹ Helmholtz Zentrum Berlin für Materialien und Energie GmbH, Institut für Si-Photovoltaik, Schwarzschildstr. 8, D-12489 Berlin, Germany

² Helmholtz-Zentrum Hereon GmbH, Max-Planck-Str. 1, D-21502 Geesthacht, Germany

E-mail: dittrich@helmholtz-berlin.de

Received 23 August 2022, revised 8 November 2022

Accepted for publication 30 November 2022

Published 12 December 2022



CrossMark

Abstract

Numerous electronic transitions in polycrystalline chemical vapor deposition diamond with characteristic nucleation and growth sides were obtained by highly sensitive surface photovoltage (SPV) spectroscopy in dc (Kelvin probe), ac (modulated) and ac (transient) regimes from near infrared to deep ultraviolet. In the dc regime, defect transitions D1 to D8 were detected at 0.8–0.9, 1, 1.37, 1.78, 2.27, 3.15, 4.2 and 5.42 eV, respectively. Hints for more transitions were found for measurements in the ac (modulated) regime in the range near D3. SPV measurements in the ac (transient) regime showed the importance of disorder for relaxation of SPV signals excited at different photon energies. Phonon assisted transitions were observed at $E_g - E_x - h\nu_{LA,LO}$, $E_g - E_x + h\nu_{LA,LO}$ and $E_g - E_x + h\nu_{TO}$. The developed SPV techniques are suitable for applications in research and quality control not only for diamond but also for any other semiconductor with ultra-wide bandgap.

Keywords: diamond, ultra-wide bandgap, defect states, electronic transitions, surface photovoltage

(Some figures may appear in colour only in the online journal)

1. Introduction

Due to its unique properties as a semiconductor with an ultra-wide bandgap (indirect bandgap of 5.47 eV [1]), diamond has a great potential for emerging applications in electronics [2, 3], optoelectronics [4], bio sensors [5], spintronics [6, 7], photocatalysis [8] and so on. For example, illumination with

ultraviolet (UV) light can provide solvated electrons for selective reduction of aqueous CO₂ to CO [9, 10], fluorescent nitrogen vacancy (NV) centers in diamond enable high-performance detection of vacuum and extreme UV as well as x-rays [11] and the charge state of NV centers can be controlled with in-plane Al-Schottky junctions [12].

Electronic states in the bandgap can play a decisive role in devices. Defect states in the bandgap of a semiconductor are often characterized by measuring electronic transitions between localized defect states and delocalized states from which charge transport or charge carriers is possible. Monitoring and control of electronic defect states in the bandgap of diamond is important for further development and for getting a deeper understanding of the role of defects in diamond related

* Author to whom any correspondence should be addressed.



Original content from this work may be used under the terms of the [Creative Commons Attribution 4.0 licence](https://creativecommons.org/licenses/by/4.0/). Any further distribution of this work must maintain attribution to the author(s) and the title of the work, journal citation and DOI.

devices and their dependence on technological processes. There is a demand for defect characterization in diamond by highly sensitive techniques for research and routine work. Surface photovoltage (SPV) (see, for example [13, 14], and references therein) techniques based on a perforated electrode and a charge amplifier allow to characterize semiconductors with ultra-wide bandgaps over wide ranges of photon energies and time domains [15].

Defect states in diamond can be caused by strain and disorder at grain boundaries, point defects in the crystal lattice or surface defects. Structural defects at grain boundaries lead to a large fraction of sp^2 bonded carbon atoms and disorder in diamond [16–18]. The concentration of hydrogen correlates with the grain size what gives evidence for passivation of dangling bonds (dbs) at grain boundaries of diamond [19]. In nanocrystalline diamond, defects at grain boundaries dominate electronic transitions from defect states in the bandgap. For example, onsets of absorption at 0.8 and 4.4 eV were attributed to transitions from π to π^* states introduced by sp^2 bonded carbon atoms and to transitions to conduction band tails caused by local disorder, respectively [20], as shown by photoconductivity. Furthermore, a quenching of photocurrent was observed at a photon energy of 3.3 eV [20]. Onset energies were obtained by photocurrent measurements on boron doped nanocrystalline diamond at 4.1 eV (valence to conduction band tails of disordered sp^3 bonded carbon atoms), at energies around and below 1 eV (π to π^* states introduced by sp^2 bonded carbon atoms) and at 3.2, 2.4, 2.3 and 2.0 eV (also called pseudo gap, caused by π to σ^* transitions whereas σ^* refer to tetrahedrally bonded carbon atoms in the grain boundaries [20]) depending on boron doping [21]. Natural type IIb diamonds are boron doped, resulting in p-type conductivity, and have an ionization energy of 0.373 eV [22]. In boron doped nanocrystalline diamond, the activation energy decreased strongly for high acceptor densities [21]. Furthermore, the threshold at 1 eV is independent of hydrogenation or oxidation and related to the grain boundaries and can be passivated with hydrogen [23].

Diamond layers prepared by chemical vapor deposition (CVD) are usually polycrystalline. In CVD diamond, transitions below the bandgap are caused by defects in the crystalline bulk and in the amorphous regions at the grain boundaries that result in onset energies of about 1 eV [24]. A transition at 1.7 eV results from substitutional nitrogen which is a deep donor being present in nominally undoped CVD diamond [24, 25]. The typical nitrogen donor absorption band is partially masked by the 1 eV band in CVD diamond [25]. Nominally undoped CVD diamond shows absorption bands which set on at 1, 2.3, 3.3 and 4.2 eV [25]. A shoulder was observed at 2.2 eV in photoconductivity spectra of CVD diamond and has been attributed to the single-substitutional nitrogen defect whereas a transitions with an onset at 1.3 eV disappeared after oxidation [26]. In nitrogen doped CVD diamond, energy levels were detected at 2.3–2.4 and 4.7 eV whereas their arbitrary density increased with increasing nitrogen concentration and their full widths at half maximum were hundreds of meV broad [27]. In addition, energy levels at 1.6 and 4.0 eV could be distinguished for nominally undoped CVD diamond [27]. The level at 4.0 eV can be related to deep

hole traps with an energy of about 1.4 eV above the valence band maximum in CVD diamond [24]. For comparison, defect states were observed in type IIb natural diamond by photoelectron yield spectroscopy at 2.0 and 4.1 eV below the conduction band minimum [28]. A defect level with an onset at 1.9 eV below the conduction band minimum was observed by photocurrent spectroscopy on a diamond crystal of type Ib [29]. Furthermore, trapping/de-trapping can cause drastic changes in transport phenomena as recently shown by transient SPV measurements without and with bias light [30].

Defects related to sp^2 bonded carbon atoms can also form at diamond surfaces and contribute to band bending and noise [31]. Calculations by density functional theory showed the formation of a primal C=C acceptor level at 1.78 eV above the valence band maximum and of states related to surface bands due to hydrogenation up to about 1.6 eV below the conduction band minimum [31]. In nominally undoped diamond the surface Fermi-level is pinned at about 1.7 eV below the conduction band minimum [24].

There were only very few attempts to apply spectral dependent SPV measurements for the characterization of diamond in the past. An onset of SPV signals was found at 5.47 eV [32] and some signals were obtained for excitation below the bandgap [33]. A spectral range from about 0.8–5.8 eV was covered and a high sensitivity was reached by applying transient SPV spectroscopy on a diamond single crystal whereas several phonon and exciton assisted transitions were distinguished near the bandgap and defect related transitions were found at 1.0, 3.1 and 1.8 eV [30].

Regarding previous characterization of electronic transitions in diamond, one shall keep in mind that transition energies can sensitively depend on the measurement technique and on the measurement conditions. Therefore, very different regimes of SPV measurements were performed with the identical electrode on the same position of a diamond sample in this work. The three complementary regimes of SPV measurements applied in this work were (a) dc (Kelvin probe), (b) ac (modulated) and (c) ac (transient) regimes. A polycrystalline CVD diamond window was chosen as a sample for demonstrating the high sensitivity and reliability of SPV for the characterization of transition energies in diamond from near infrared to deep UV. An advantage of a polycrystalline CVD diamond window was that numerous electronic transitions appeared across the overall spectral range due to defect states in grain boundaries and in crystallites. Furthermore, the density of grain boundaries was very high at the nucleation side and very low at the growth side of the polycrystalline CVD diamond window so that the specific influence of charge separation across very small and large grains could be studied.

2. Experimental

Polycrystalline diamond samples (thickness 0.1 mm, area $1 \times 1 \text{ cm}^2$) as used for window applications were prepared by CVD (Diamond Materials GmbH, type II diamond, hydrogen content below 1000 ppm, silicon and nitrogen content below

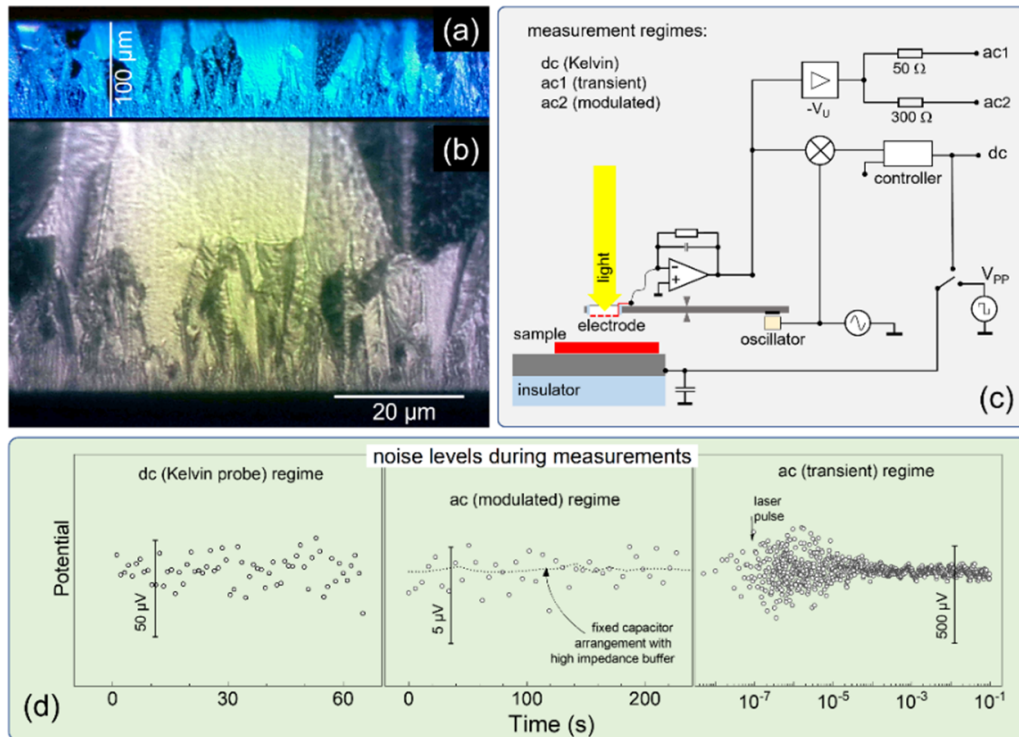


Figure 1. Cross section of the polycrystalline diamond sample (a), zoomed closer on the nucleation side (b), schematic set-up of electronics for dc (Kelvin probe), ac (transient) and ac (modulated) regimes (V_{pp} denotes the test signal) (c) and noise levels characteristic for the measurements of overview spectra in the three regimes (d). For comparison, the dotted line marks the noise level for modulated measurements in the fixed capacitor arrangement with a high impedance buffer.

10 ppm). Figure 1(a) shows a cross section, obtained by transmitted light microscopy, of the polycrystalline diamond sample. The characteristic nucleation and growth sides with sizes of crystallites of the order and below 1 μm (see also figure 1(b)) and about 10–50 μm, respectively, are clearly distinguished.

SPV measurements were performed at room temperature (25 °C) in air. For the SPV measurements, a perforated electrode (coated with gold, diameter 7 mm) and an electromagnetic oscillator were mounted at the opposite sides of a steel bar fixed in the center by a knife-edge (see figure 1(c)). The resonance frequency of the steel bar was 1.05 kHz. This relatively high frequency allowed for a comfortable construction at further reduction of noise. The oscillator with the electrode, charge amplifier (resolution time 10 ns), controller and source of the test signal were realized in one set-up (electronics by Elektronik Manufaktur Mahlsdorf) for measurements in the dc (Kelvin-probe) and ac (modulated and transient) regimes. The electrode oscillated at the resonance frequency in the dc regime and was fixed in the ac regimes. The sample holder (stainless steel) was isolated to ground. In the dc regime, the potential was applied to the sample holder and measured signals corresponded to negative contact potential differences ($-\Delta CPD$). A light induced change of $-\Delta CPD$ corresponds to a change of SPV.

SPV signals in the ac regimes were calibrated with a periodic test signal (1 V peak-to-peak) applied to the sample holder. The resulting amplification factor was adjusted to 10

by varying the distance between the electrode and the sample surface with a micrometer screw. The dc, modulated and transient SPV signals were measured with a multimeter (HP 34401A), a lock-in amplifier (EG&G 7260) and an oscilloscope card (Gage, CSE 1622-4GS), respectively.

A quartz prism monochromator (SPM2, Carl Zeiss Jena) was used for measurements at photon energies (E_γ) of up to 6 eV (Xe lamp for illumination) or up to 4 eV (halogen lamp for illumination). Incidentally, the advantage of a halogen lamp is the absence of spectral lines in comparison to a Xe lamp. The light spot was adjusted with a quartz lens at a wavelength (λ) of 250 nm (E_γ about 4.96 eV) on the electrode for measurements with the Xe lamp. The total measurement time of a spectrum in the dc and ac (modulated) regimes was about 30 min. Consecutive measurements were performed in the dc regime in order to get information about ongoing charging. The measurements started at the lowest E_γ of a spectrum. The entrance slit of the monochromator was closed during the time when the monochromator went back to the lowest E_γ between two consecutive measurements.

A tunable Nd:YAG laser (EKSPLA, NT230-50, equipped with a spectral cleaning unit, duration time of laser pulses 3–5 ns, range of wavelengths 213–2200 nm) was used for excitation of SPV signals in the transient regime. The photon flux was kept nearly constant (see also [34] for more details) between about 1.2 and 4.2 eV by using a motorized tunable beam expander (6-BE-TX2.5-0355-M, Altechna motex) in combination with reflection-based intensity filters in a

motorized filter wheel. At photon energies below 1.2 and above 4.2 eV, the photon flux was limited by the laser intensity and the minimum zoom factor for the beam expander (2.5) and no filter was used. For the transient SPV spectroscopy measurements, the repetition rate of the laser pulses was 0.25 Hz and ten transients were averaged at any given measurement point. Samples were flipped for changing illumination from the nucleation to the growth sides.

Characteristic noise levels of corresponding dark measurements are shown in figure 1(d) for the applied measurement conditions. Due to the relatively high vibration frequency of the steel bar and due to the placement of the charge amplifier close to the electrode, the noise level in the dc (Kelvin probe) regime was of the order of $30 \mu\text{V}$ during spectral dependent measurements (measurement time of a full spectrum below 30 min). The noise level was about $3 \mu\text{V}$ for measurements in the ac (modulated) regime with the charge amplifier. In the near infrared to visible range, some modulated SPV measurements were performed at a very low noise level with a high impedance buffer in the fixed capacitor arrangement using an electrode coated with $\text{SnO}_2:\text{F}$ and a mica spacer between the electrode and the sample surface [35]. Noise levels below $0.5 \mu\text{V}$ were achieved for moderate averaging by amplifying the signals by a factor of 10 in the high impedance buffer (Elektronik Manufaktur Mahlsdorf) and placing the battery close to the high impedance buffer. For transient measurements with the charge amplifier, the noise levels were about $500 \mu\text{V}$ at the shortest times and decreased below $100 \mu\text{V}$ at times longer than 0.1 ms due to the logarithmic read-out with increasing time intervals for averaging [36].

3. Results and discussion

3.1. SPV spectroscopy in the dc (Kelvin probe) regime

Due to charging and discharging of electronic states, SPV signals depend also on the measurement regime. For example, several processes resulting in SPV signals with opposite signs can take place in one sample at the same photon energy and time. For demonstrating, figure 2 shows two sequences of $-\Delta\text{CPD}$ signals measured for illumination from the nucleation side at decreasing excitation wavelengths whereas λ was reduced every 100 s. The first sequence was measured without any filter. For the second sequence, a cut-on filter (cut-on wavelength 900 nm) was placed behind the exit slit of the monochromator in order to reduce the influence of straylight at shorter wavelengths (see also discussions of different roles of straylight in [14, 37]). Incidentally, straylight contains photons of a broad spectrum and can therefore induce offsets and influence values of SPV signals or may even lead to additional peaks in SPV spectra.

The entrance slit was opened at 3100 nm after the first 100 s. After opening the entrance slit, $-\Delta\text{CPD}$ changed towards more positive values by up to about 37 mV for the sequence without filter. In contrast, the slope of $-\Delta\text{CPD}$ changed to less negative for the sequence with filter. Therefore, straylight is important for the formation of SPV signals.

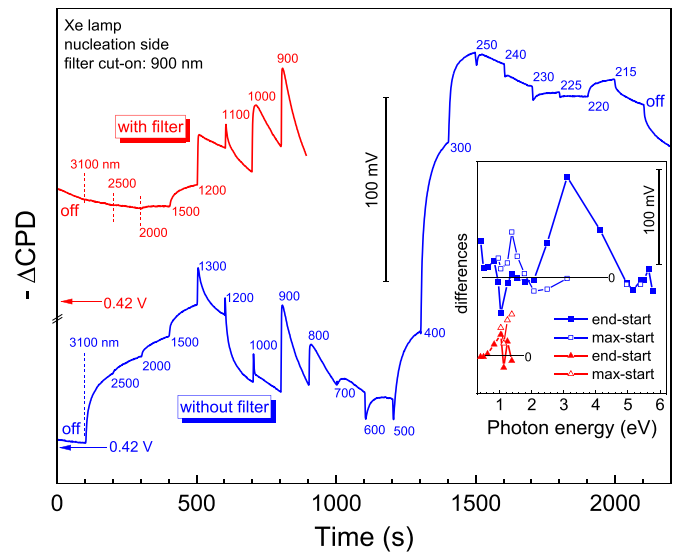


Figure 2. Sequences of the contact potential difference under illumination with decreasing wavelengths of a Xe-lamp (100 s for each interval) for illumination without a filter (blue line, full range of wavelengths) and with a cut-on filter at 900 nm (red line). The values of the wavelengths are given as small numbers near the time when changing to the corresponding wavelength. The slit of the monochromator was closed during the first 100 s (off). The sequence measured with a filter was shifted up by 80 mV for separating it from the sequence measured without filter. Furthermore, the measurement with a filter was performed after the measurement without a filter resulting in an additional up-shift due to slow relaxation of some charge carriers separated before. The insert shows spectra deduced from the differences of $-\Delta\text{CPD}$ measured at the end and at the beginning or in the maximum of a sequence as function of photon energy.

After changing λ to 2500, 2000 and 1500 nm, $-\Delta\text{CPD}$ increased by 9, 11 and 19 mV, respectively, for the sequence without filter. For the sequence with filter, the changes of $-\Delta\text{CPD}$ increased from 2 mV (2000 nm) to 11 mV (1500 nm), i.e. a transition causing positive SPV signals set on.

For the sequence without filter and after changing λ to 1300 nm, $-\Delta\text{CPD}$ increased towards more positive values by about 20 mV and, after several s, $-\Delta\text{CPD}$ started to change towards more negative values by more than about -25 mV at 100 ns. Furthermore, after changing λ to 1200 nm, $-\Delta\text{CPD}$ changed more rapidly towards more positive values by about 10 mV and towards more negative values up to -45 mV afterwards. The similar behavior was observed after changing λ to 1000 nm but with less change of $-\Delta\text{CPD}$ to more negative values. This means that, aside the process resulting in positive SPV signals, a second process causing negative SPV signals with slower dynamics sets on. The similar process was observed for measurements with the filter, however, the change of $-\Delta\text{CPD}$ to more negative values dominated only at 1100 nm (instead of 1300, 1200 and 1000 nm for the measurements without a filter). For excitation at 900 nm, the behavior was rather similar for measurements without and with filter.

After changing λ to 600 nm (at 1100 s in figure 2), $-\Delta\text{CPD}$ changed rapidly towards more negative values by about -15 mV and towards more positive values of the similar

magnitude within the following time. Therefore, another process of charge separation causing negative SPV signals at shorter time to set on.

After changing λ to 500 nm, $-\Delta\text{CPD}$ changed rapidly towards more negative values by about -10 mV and towards more positive values by more than 40 mV within the following time. After changing λ to 400 nm, $-\Delta\text{CPD}$ changed rapidly towards more negative values by a small amount of about -2 mV and towards more positive values by more than 100 mV within the following time which was the strongest change in the whole sequence. After changing λ to 300 nm, $-\Delta\text{CPD}$ changed rapidly towards more positive values by about 50 mV. Therefore, the most dominating process of charge separation caused positive SPV signals, sets on between 500 and 400 nm and decreased at λ shorter than about 300 nm.

After changing λ to 250 nm, $-\Delta\text{CPD}$ changed rapidly towards more negative values within the first seconds, to more positive values within the following 10–20 s and to more negative values again at longer times. This means that a superposition of more than two processes occurred. A qualitatively similar behavior appeared after changing to 240 nm whereas the slow change towards more negative values of $-\Delta\text{CPD}$ disappeared after changing λ to 230 nm.

After changing λ to 225, 220 and 215 nm, $-\Delta\text{CPD}$ changed towards more negative, more positive and more negative values, respectively, without signatures of more than one processes of charge separation. Therefore, the direction of dominating charge separation changed in the range of the bandgap.

The insert of figure 2 summarizes the sequences as spectra of the differences of $-\Delta\text{CPD}$ at the end or at the maximum and at the beginning of a sequence. The change towards more negative values sets on at 0.82 and 1.03 eV and the negative maxima were reached the about 1.03 and 1.13 eV for measurements with and without the cut-on filter. This gives an impression about the uncertainty in determining transition energies by SPV spectroscopy. Other transitions towards more negative values set on at about 1.38 and 3.2–3.5 eV. The change towards more negative values above 5.64 eV seems to be caused by the strong decrease of the light intensity at these photon energies. Changes towards more positive values appeared below 1 eV, around 2 eV, and around 5.2 and 5.5 eV.

Figure 3 shows spectra of $-\Delta\text{CPD}$ under illumination with a Xe-lamp (a) and a halogen lamp (b) under illumination from the nucleation and growth sides for several consecutive measurements (a) and the 3rd measurement (b). The values of $-\Delta\text{CPD}$ and their changes obtained at the beginning of the consecutive spectra give information about charging.

For three consecutive measurements under illumination from the nucleation side with the Xe-lamp (figure 3(a)), the values of $-\Delta\text{CPD}$ at the beginning were positive and amounted to about 0.62, 0.66 and 0.62 V (1st, 2nd and 3rd, respectively). For comparison, $-\Delta\text{CPD}$ was about 0.6 V for the bare sample holder. In contrast, the values of $-\Delta\text{CPD}$ at the beginning were negative and amounted to about -1.04 , -1.00 and -0.89 V (1st, 2nd and 3rd, respectively) under illumination

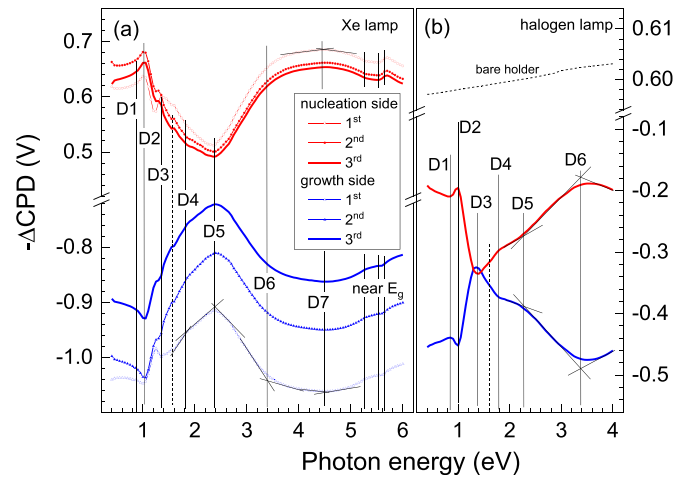


Figure 3. Spectra of the light-induced change of the contact potential difference under illumination with a Xe-lamp (a) and a halogen lamp (b) for the polycrystalline diamond sample illuminated from the nucleation and growth sides (red and blue lines, respectively). Three consecutive measurements are shown for illumination with the Xe lamp (increasing thickness of the lines with increasing number of measurement) and the third measurement for illumination with the halogen lamp. The dashed black line shows the spectrum of the bare sample holder for comparison. The vertical solid lines mark energies with characteristic changes in $-\Delta\text{CPD}$. Transitions below the bandgap are denoted by D1–D6. The dashed line denotes a transition characterized by a very weak shoulder.

from the growth side. This means that the growth side was charged negatively and that the negative charge decreased under illumination with the Xe lamp during the measurement of a spectrum whereas the charge at the nucleation side did change less. On the other side, the nucleation side was charged more positively which can be related to a higher density of grain boundaries and/or of specific surface states at the nucleation side.

After illumination with the Xe lamp, the crystal was stored in the dark overnight before measurements were performed with the halogen lamp. Under illumination with the halogen lamp, the values of $-\Delta\text{CPD}$ at the beginning of the 2nd and 3rd spectra were about -0.1 and -0.19 V (illumination from the nucleation side, not shown) and about -0.40 and -0.45 V (illumination from the growth side), respectively. This means that both sides were charged negatively, whereas the negative charge was larger at the growth side. Furthermore, the negative surface charge increased at both surfaces during the measurement of a spectrum under illumination with the halogen lamp. Therefore, the charge at surfaces of CVD diamond depends sensitively on the illumination spectrum and history.

In the spectra of $-\Delta\text{CPD}$, the strongest changes appeared near 1.0 eV. At this photon energy, the $-\Delta\text{CPD}$ started to change towards more negative for illumination from the nucleation side independently whether illumination was performed with a Xe or halogen lamp. In contrast, the values of $-\Delta\text{CPD}$ started to change towards more positive for illumination from the growth side. This indicates that excitation of the transition setting on at 1 eV led to a preferential separation of

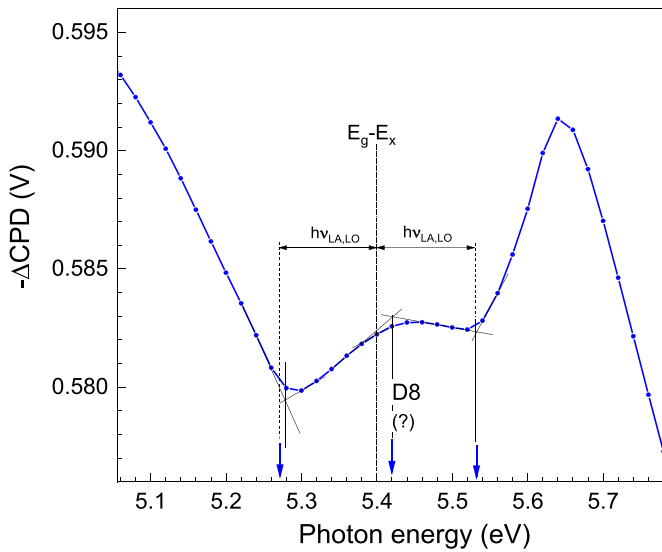


Figure 4. More detailed spectrum of $-\Delta\text{CPD}$ above 5.06 eV (illumination from the nucleation side).

photogenerated electrons towards the nucleation side, i.e. to an increase of negative charge at the nucleation side and a reduction of negative charge at the growth side.

A Xe lamp has strong spectral lines in the near infrared region. Therefore, transitions in the near infrared region will be analyzed for spectra obtained for illumination with the halogen lamp. Around 0.8–0.9 and 1.4 eV, the values of $-\Delta\text{CPD}$ changed towards more negative (more positive) for illumination from the growth side (nucleation side). The transitions near 0.8–0.9, 1.0 and 1.4 eV are denoted by D1, D2 and D3 in the following.

A change in the slope in ΔCPD spectra is usually assigned to the onset of a new transition leading to a change in charge separation. For illumination from the growth side (nucleation side), the slopes of the ΔCPD spectra became less negative (positive) at about 1.8 eV, more negative (positive) at about 2.3 eV and changed from negative (positive) to positive (negative) at about 3.3 eV. The transitions at 1.8, 2.3 and 3.4 eV were assigned to D4, D5 and D6, respectively. A slight shoulder was observed around 1.6 eV, but regarding the given data it cannot be assigned as a well pronounced transition (see the dashed lines in figure 3). The transitions D1 to D6 appeared also for illumination with the Xe lamp whereas they were partially influenced by spectral lines between 1.2 and 1.4 eV and between 2.5 and 2.7 eV. An additional transition at about 4.5 eV (denoted as D7) was observed for illumination with the Xe lamp (see figure 3(a)).

Figure 4 gives a more detailed spectrum of $-\Delta\text{CPD}$ for illumination from the nucleation side in the range of the bandgap. Four well pronounced features appeared at 5.28, 5.42 and 5.53. The transitions at 5.28 and 5.53 eV can be assigned to the transitions at $E_g - E_x - h\nu_{\text{LA,LO}}$ and $E_g - E_x + h\nu_{\text{LA,LO}}$, respectively, where E_g , E_x and $h\nu_{\text{LA,LO}}$ denote the indirect bandgap (5.47 eV), the binding energy of the indirect exciton (0.07 eV) and the energy of the longitudinal optical and

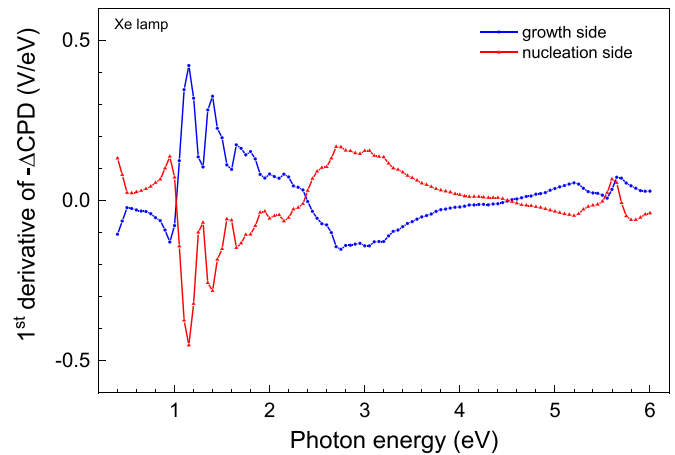


Figure 5. First derivative of the $-\Delta\text{CPD}$ spectra (3rd measurement) for illumination from the nucleation and growth sides (red and blue lines, respectively).

acoustical phonons (0.132 eV), respectively [1]. The feature at 5.42 eV was also described in absorption analysis but it was not assigned to a transition assisted by phonons [1]. It seems reasonable to assume that the signature at 5.42 eV belongs to a defect transition (assigned by D8). Incidentally, the change of $-\Delta\text{CPD}$ towards less positive values at photon energies above 5.6 eV was caused by the strong decrease of the light intensity.

The $-\Delta\text{CPD}$ spectra for illumination from the growth and nucleation sides were for the most part of the spectra mirror symmetric. The mirror symmetry can be also well seen in the derivatives of the spectra shown in figure 5. A deviation from the mirror symmetry was observed at photon energies higher than about 5.5 eV. Therefore, the mechanisms of photogeneration, charge separation and relaxation were practically on the illuminated side for low absorption coefficients. In the range of the bandgap, the absorption coefficient increases drastically so that absorption and charge separation within small crystallites at the nucleation side became more dominant for the measurements under illumination from the nucleation side.

3.2. Transitions probed under ac (modulated) SPV spectroscopy

Modulated SPV signals arise when charge separation and relaxation can follow the modulation. Modulated overview spectra of the in-phase (X) and phase-shifted by 90° (Y) signals are depicted in figure 6(a) for the polycrystalline diamond sample under illumination with a halogen lamp from the growth side. Incidentally, the X and Y signals are caused by the fast and slow responses, respectively, in relation to the modulation period. Furthermore, in the case of preferential separation of photogenerated electrons towards the surface (or holes towards the bulk), the X and Y signals are negative and positive, respectively, which follows from the analysis with a lock-in amplifier (see for more details also [14]). Transitions

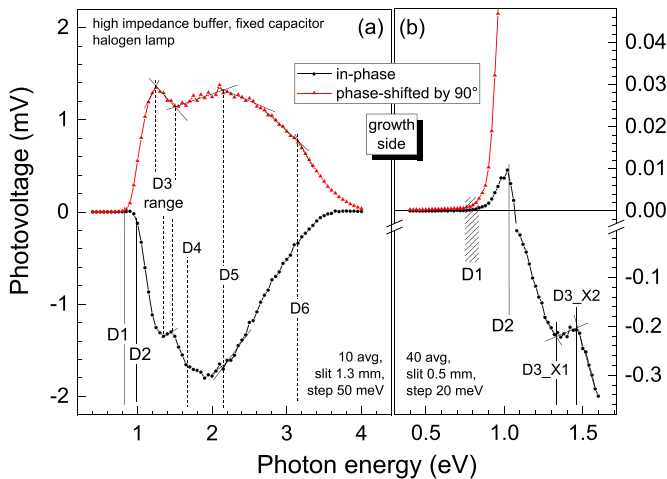


Figure 6. Modulated SPV spectra of the in-phase (black) and phase-shifted by 90° (red) signals for the polycrystalline diamond sample under illumination with a halogen lamp from the growth side ((a): overview spectrum, (b): spectrum near infrared with reduced entrance and exit slits of the monochromator and reduced noise). For further noise reduction in the corresponding spectral range, a measurement (b) was performed with a fixed capacitor arrangement and a high impedance buffer.

at 0.8–0.9 eV (D1) and 1.0 eV (D2) were well pronounced for the phase-shifted by 90° and for the in-phase spectra, respectively. Several features appeared between about 1.2 and 1.5 eV whereas the onset energies were different for the X and Y signals, i.e. there was not one well defined feature at transition D3 (about 1.35 eV). The X-signals started to change towards less negative values at 1.33 eV and towards higher negative values at 1.46 eV (D3_X1 and D3_X2, respectively). The Y-signals started to change towards less positive values at 1.24 eV and towards higher positive values at 1.52 eV (D3_Y1 and D3_Y2, respectively). Figure 6(b) gives a closer look at the range of D1, D2, D3_X1 and D3_X2 whereas the noise was additionally reduced and the resolution and the number of data points were increased. The X and Y signals were both positive in the range of the D1 transition giving evidence for two processes of charge separation with opposite sign and rather different relaxation times. With the onset of D2, the X signals changed towards positive and changed the sign at 1.06 eV. This shows that one process of charge separation dominated for excitation at D2.

A pronounced shoulder appeared at about 1.64 eV in the spectrum of X signals. However, a feature related to this shoulder did not appear in the spectrum of the Y signals. The shoulder at about 1.64 eV in the spectrum of the in-phase signals seems to be a signature in the range of transition D4. At about 2–2.2 eV, the X and Y signals started to decrease which might be a signature for transition D5. The Y signals started to decrease stronger at photon energies above about 3.15 eV what is a signature for transition D6.

The modulated SPV spectra measured for illumination from the growth and from the nucleation sides were also highly symmetric and deviations appeared only at very low signals.

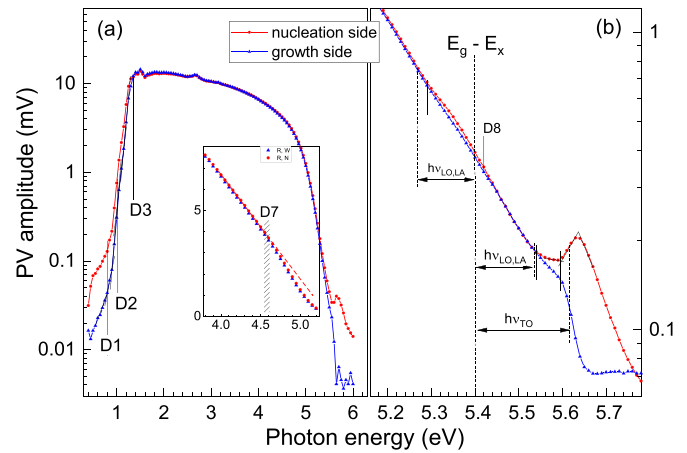


Figure 7. Overview spectra of the amplitudes of the modulated SPV for the polycrystalline diamond sample measured from the nucleation and growth sides (red circles and blue triangles, respectively) (a) and more detailed spectra measured in the region around the bandgap (b). The insert of (a) is a zoom on a linear scale in the range of D7.

Figure 7 shows the amplitude spectra for illumination from the growth and nucleation sides under illumination with the Xe lamp. At photon energies below 1.3 eV, the signals were significantly larger for illumination from the nucleation side due to increased light scattering at grain boundaries into the bulk which lead to an increased probability of light absorption. At photon energies around 0.5 eV, the signals for illumination from the nucleation side were larger by three to four than the signals for illumination from the growth side despite the maximum amplitudes were practically identical. This means that scattering of straylight had much stronger influence for illumination from the nucleation side.

Onsets of transitions D1 and D2 could be distinguished as shoulders in the amplitude spectra measured under illumination with the Xe lamp and saturation was reached near transition D3. Features near the transitions D4, D5 and D6 could not be distinguished. It seems that the high intensity of the Xe lamp and its wide spectrum of straylight strongly reduced the detection contrasts of modulated charge separation and relaxation for transitions D3–D6 on top of signals dominated by D2. Around transition D7 at 4.5–4.6 eV, the amplitude started to decrease stronger than at photon energies below. Therefore, modulated charge separation was partially quenched for light absorbed via transition D7.

Some characteristic features appeared in the region around the bandgap (figure 7(b)). The most pronounced changes in the slopes were found at about 5.53 and 5.60 eV. These transitions are relatively close to $E_g - E_x + h\nu_{LA,LO}$ (5.531 eV) and $E_g - E_x + h\nu_{TO}$ (5.615 eV) [1], respectively. Incidentally, the strong decrease of the SPV signals at photon energies above about 5.65 eV was caused by the strong decrease of the light intensity. For illumination from the nucleation side, the SPV signals started to increase stronger above 5.6 eV. In contrast, for illumination from the growth side, the SPV signals were quenched above 5.6 eV. Weak features at 5.3 and 5.42 eV

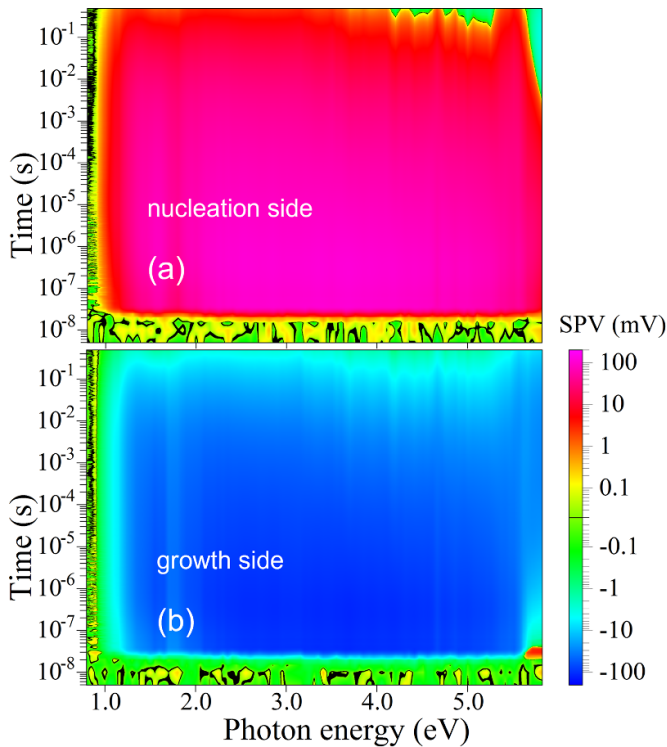


Figure 8. Contour plots of the transient SPV signals as functions of photon energy and time for polycrystalline diamond under illumination from the nucleation and growth sides ((a) and (b), respectively). Signals between -0.02 and $+0.02$ mV were discriminated in the logarithmic color scale.

in the spectrum measured under illumination from the nucleation side may be related to $E_g - E_x - h\nu_{\text{LA,LO}}$ (5.268 eV [1]) and/or at $E_g - h\nu_{\text{TO}}$ (5.315 eV [1]). The small feature at around 5.42 eV can be assigned to transition D8.

3.3. Transient SPV spectroscopy

The contour plots of the transient SPV signals, i.e. the distribution of SPV signals on a logarithmic color scale as function of photon energy and logarithmic time, are shown in figure 8 for illumination from the nucleation (a) and growth (b) sides. The SPV signals were positive for illumination from the nucleation side or negative for illumination from the growth side starting from about 1 eV over nearly the whole range in photon energy and time whereas the maxima were of the order of $+100$ or -100 mV, respectively. Therefore, the contour plots of polycrystalline diamond were dominated by charge separation via defect states with transitions energies close to 1 eV. Incidentally, the contour plots of single crystalline diamond were dominated by transitions in the range of the bandgap and signals related to defect transitions were lower by about one order of magnitude [30].

At long times, the sign changed to low negative values for excitation with photon energies above 5.6 eV for illumination from the nucleation side. In contrast, at very short times, the sign changed to low positive values for excitation with photon energies above 5.6 eV for illumination from the growth side.

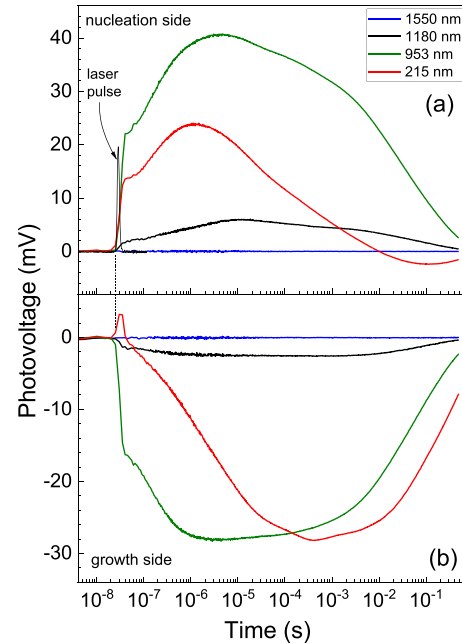


Figure 9. SPV transients excited at wavelengths of 1550 , 1180 , 953 and 215 nm (blue, black, green and red lines, respectively) for illumination from the nucleation (a) and growth (b) sides. The thin black line represents the shape of the laser pulses.

This is also demonstrated in figure 9 showing SPV transients for excitation at wavelengths of 215 as well as of 953 , 1180 and 1550 nm under illumination from the nucleation and growth sides, (a) and (b), respectively. For illumination from the growth side at 215 nm (5.767 eV), the SPV signals increased to $+3.2$ mV within the resolution time, decreased at longer times, changed the sign and increased to -1 mV in the following 20 ns and the negative maximum of -28 mV was reached after 0.4 ms. In contrast, for illumination from the nucleation side at 215 nm, the SPV signals increased to $+13.7$ mV within the resolution time, reached the maximum of 24 mV at 1 μs , started to decrease, changed the sign at about 10 ms and reached the negative maximum of -2.3 mV at about 120 ms. The positive and negative SPV signals at the shortest and longest times, respectively, for illumination from both growth and nucleation sides at 215 nm shows that there are similarities in charge separation at both surfaces independent of the size of diamond crystallites. It seems that, in comparison to the bandgap of diamond, a very low positive surface band bending caused the fast positive SPV signals whereas electrons trapped at surface states caused the negative SPV signals at long times.

Under illumination from the growth side at 1180 and 953 nm, the negative SPV signals increased within the resolution time to about -1.4 and -14.6 mV, respectively, and continued to grow up to -2.6 and -29 mV within the following 3 μs , respectively. Under illumination from the nucleation side at 1180 and 953 nm, the positive SPV signals increased within the resolution time to about 1.6 and 22 mV, respectively, and continued to grow up to 6 and 41 mV within the following 10 and 4 μs , respectively. For excitation at photon

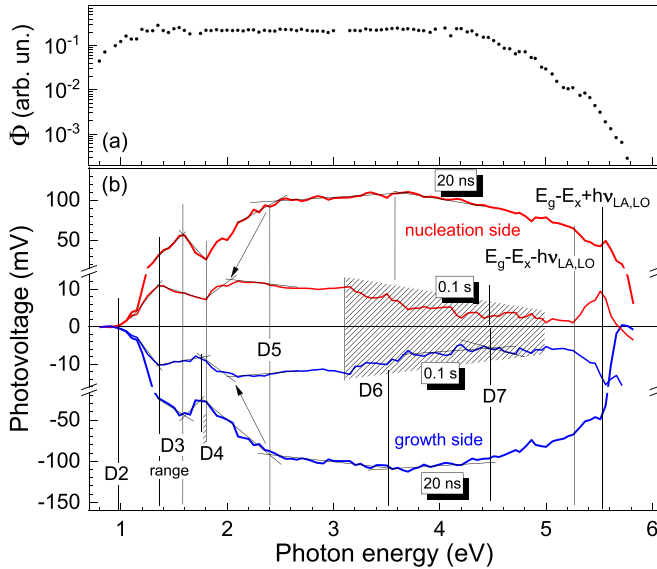


Figure 10. Spectrum of the photon flux (a) and SPV spectra deduced at 20 ns (thick lines) and 0.1 s (thin lines) after excitation of the polycrystalline diamond sample from the nucleation and growth sides (red and blue, respectively) (b). Vertical lines mark transition energies distinguished. The hatched area marks the region of increased noise.

energies below the bandgap, the shapes of the SPV transients were rather similar but not identical under illumination from the growth and nucleation sides.

Figure 10 shows the spectra of the photon flux (a) and of the SPV spectra obtained at times of 20 ns and 0.1 s after excitation for illumination from the nucleation and growth sides (b). SPV signals set on between 0.95 and 1.0 eV (transition D2). Incidentally, the sensitivity was not high enough to detect unambiguously signals between 0.8 and 0.9 eV (D1). At 1.58 and 1.36 eV (D3 range), SPV signals measured after 20 ns and 0.1 s, respectively, started to decrease, i.e. the SPV signals became less positive for illumination from the nucleation side and less negative for illumination from the growth side. At 1.8 eV, the SPV signals started to increase, i.e. the signals became more positive for illumination from the nucleation side and more negative for illumination from the growth side.

At about 2.4 eV (transition D5), the increase of the SPV signals reduced so that well pronounced kinks appeared in the spectra obtained after 20 ns. With increasing time, these kinks shifted towards lower photon energies and became little peaks with maximum at about 2.0 eV obtained after 0.1 s. At about 3.7 eV (transition D6), the SPV signals started to decrease in the spectra obtained after 20 ns. With increasing time, this starting point of the decrease shifted to lower photon energies up to about 3.1 eV in the spectra obtained after 0.1 s. A signature related to transition D7 could not be distinguished for the spectra obtained after 20 ns. At photon energies of about 4.5 eV, a slight increase of the SPV signals was observed in the spectra obtained after 0.1 s.

For the spectra deduced after 0.1 s, the noise level was much higher between about 3.1 and about 5 eV in comparison to the ranges below 3.1 and above 5.0 eV. This intriguing fact gives

evidence that charge separation and relaxation can be unstable under certain excitation conditions. It seems that this is the case when exciting in the range with overlap of transitions related to D5 and D6. Incidentally, a partial quenching of the photoconductivity was observed at 3.3 eV for hydrogen rich nanocrystalline diamond [20] as well as at around 2.7 eV for lateral hydrogen/oxygen terminated in-plane junctions [38]. Incidentally, the hydrogen content of the investigated CVD diamond was also relatively high (below 1000 ppm). The transition at 2.7 eV was explained by defect states at about 1 eV above the valence band maximum and relatively large local potential fluctuations of up to more than 0.1 V have been observed [38]. We believe that charge separation is highly sensitive to local fluctuations of the Fermi-level or potential at or near grain boundaries under illumination at photon energies above 3.1 eV.

In the region around the bandgap, signatures could be distinguished at 5.27 and 5.53 eV which can be assigned to the $E_g - E_x - h\nu_{LA,LO}$ (5.268 [1]) and to $E_g - E_x + h\nu_{LA,LO}$ (5.531 eV [1]) transitions, respectively. For comparison, additional transitions at 5.32 and 5.48 eV, which were related to the $E_g - E_x - h\nu_{TA}$ and to $E_g - E_x + h\nu_{TA}$, respectively, have been observed in the transient SPV spectra of high quality single crystalline diamond [30]. It seems, since the SPV signals were up to about ten times larger for the transient SPV measurements on single crystalline diamond, that the sensitivity was not high enough to detect the transitions at 5.32 and 5.48 eV on polycrystalline CVD diamond.

3.4. Comparison and discussion of transition energies

Similar transition energies were observed with different sensitivity for SPV measurements in the dc (Kelvin probe), ac (modulated) and ac (transient) regimes and the energies of some transitions depended on the regime. Figure 11 summarizes the transitions observed by SPV measurements in polycrystalline CVD diamond. In the following discussions, illumination from one side will be considered since the SPV signals were symmetric for illumination from the nucleation and growth sides.

For measurements in all three regimes, the most dominant transition was that at about 1 eV (D2). The energy of the D2 transition was practically constant and did not depend on the measurement regime. The transition D2 can be related to the onset of electron excitation from π to π^* states [21]. The signs of the SPV signals were positive for the D2 transition under illumination from the nucleation side in the ac (modulated) and ac (transient) regimes. In the dc (Kelvin probe) regime, the signs of the SPV signals were also positive for the D2 transition under illumination from the nucleation side if blocking straylight at higher photon energies with a filter but the sign changed from positive negative during illumination if not blocking the straylight (see figure 2). As consequence, the sign of the SPV signals related to the D2 transition was negative in the dc overview spectra under illumination from the nucleation side. This shows that the redistribution in space of trapped charge was very important for the formation of the SPV signals.

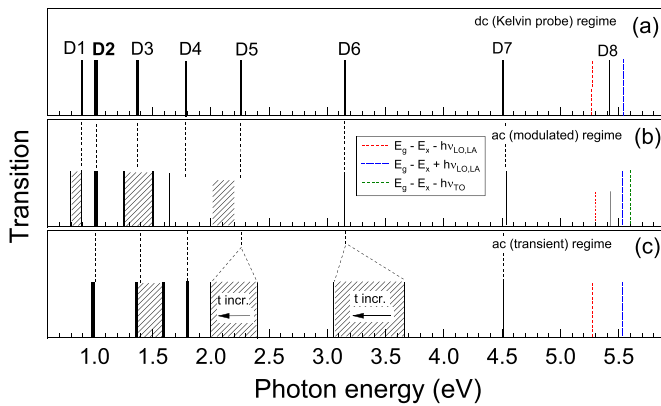


Figure 11. Summary of transitions observed in polycrystalline CVD diamond in the dc (Kelvin probe), ac (modulated) and ac (transient) regimes ((a)–(c), respectively).

Signatures were found for transition D1 (0.8–0.9 eV) by measurements in the dc (Kelvin probe) and ac (modulated) regimes whereas the sensitivity was not high enough for detection of D1 by measurements in the ac (transient) regime. The sign of the SPV signals was positive for illumination from the nucleation side in the dc (Kelvin probe) regime for measurements with and without suppression of straylight (figure 2). Furthermore, the signs of the SPV signals related to D1 and D2 were opposite for measurements in the ac (modulated) regime. Therefore, transition D1 belongs to other defects than transition D2.

The region around transition D3 (1.37 eV for measurements in the dc (Kelvin probe) regime) is intriguing since there were several different signatures in the corresponding spectral range for measurements in the ac (modulated) regime. The corresponding onset energies depended on the analysis X or Y signals. Since the X and Y signals belong to fast and slow response times in relation to the modulation frequency, the corresponding defect states have a relatively broad energy distribution. In addition, there were two different onset energies for signals getting less negative or more negative (X signals) or less positive or more positive (Y signals) for illumination from the growth side with a halogen lamp (see figure 6). There were also two different onset energies in the spectral range of the D3 transitions for measurements in the ac (transient) regime. Therefore, it seems that several transitions occurred between about 1.25 and 1.6 eV and that the duty cycle of the measurement regime (for dc, 1:1 for modulated, $1:10^8$ – $1:10^9$ for transient measurements) plays an important role for detection of transitions. Much more detailed experiments will be required for getting a deeper understanding of the defect states in this range, what was behind the scope of the work.

Transition D4 (1.78–1.8 eV) was well detected in the dc (Kelvin probe) and ac (transient) regimes. A shoulder appeared only around 1.65 eV in the X signals measured with a halogen lamp and might give a hint for a signature of D4, but this is under question. The transition energy of D4 can be assigned to a bulk defect.

Transitions D5 (2.27 eV, dc) and D6 (3.15, dc) could be well detected for measurements in the dc (Kelvin probe) regime but not for both in-phase and phase-shifted by 90° signals in the ac (modulated) regime. In the ac (transient) regime, the energies of transitions D5 and D6 shifted to lower values with increasing relaxation time. The ranges of onset energies changed over about 0.2 and 0.3 eV for transitions D5 and D6, respectively. This gives evidence that transitions D5 and D6 are related to a disordered phase at grain boundaries where the density of states decreases with increasing energy difference to the transport level. This also means, if regarding to $\pi\sigma^*$ transitions [21], that photogenerated electrons can be separated along the disordered grain boundaries at energies independently from the crystalline phase. Transition D7 can be considered as the excitation of electrons from the valence and to conduction band tails in the grain boundaries [20]. The origin of transition D8 is unclear.

In the following, ideas for a basic concept of interpretation of defect related SPV signals in polycrystalline diamond will be drawn. Most defects are caused by disorder at grain boundaries in polycrystalline diamond. The density of grain boundaries is very high at the nucleation side and very low at the growth side. The occupation of defect states within the corresponding local gradients of defects shall be considered as the main driving force for the evolution of dc, ac modulated and ac transient SPV signals. Charge separation can be driven by gradients of accessible states acting as local sinks and by electrostatic repelling or attracting charge carriers due to trapped charge carriers (see also figure 12(a)).

Charge transfer and back transfer rates to defect states at grain boundaries have a tremendous influence on the formation of SPV signals at different time scales and can even cause opposite signs of SPV signals measured in different regimes. For example, for excitation at transition D2 from the nucleation side, the dc SPV signals were negative but the ac modulated and ac transient SPV signals were positive in the spectra. In addition, time dependent measurements of dc SPV signals around D1 and D2 transitions depended strongly on straylight. Regarding to [20], transitions D1 and D2 can be related to transitions between π states and un-occupied states of dbs and occupied states of dbs and π^* states (see also figure 12(b)).

The density of π and π^* states is high so that charge carriers can be transferred by hopping inside the bands of π and π^* states. On the other side, the density of dbs is low so that charge transfer between db states by tunneling can be neglected. The density of available states is higher in regions where several grain boundaries come together. This means that excited electrons and holes move preferentially towards internal grain boundaries oriented in parallel to the surface (A in figure 12(a)). Usually, electrons move faster than holes so that positive SPV signals appear at short times under excitation from the nucleation side. At longer times, the positive SPV signals decrease due to ongoing hole transfer. After switching off illumination, electrons separated in space relax faster than holes so that the SPV signals at the D2 transition change the sign to negative due to remaining separated holes. This

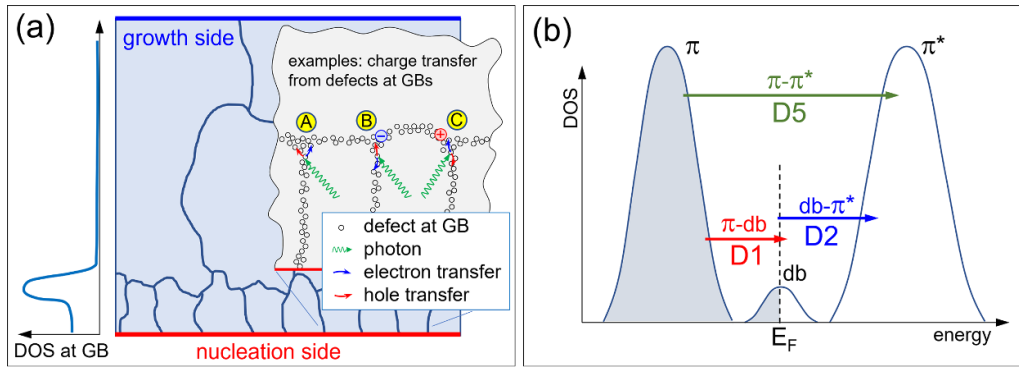


Figure 12. Idealized cross section of polycrystalline diamond with grain boundaries (GBs), density of states at GBs (left) and examples for charge transfer from defect states (A: transfer to unoccupied states, B and C: transfer influenced by trapped negative and positive charge, respectively) (a) and idealized densities of states for db, π and π^* states with π -db (D1), db- π^* (D2) and π - π^* (D5) transitions (b). Charge carriers can be transferred by hopping inside the π and π^* bands.

has been observed for time dependent dc SPV signals (excitation, for example, at 1200 nm) and for spectra. Under the influence of straylight, more of the deepest states are permanently occupied so that de-trapping times decrease and relaxation becomes faster. Under ac modulated and repetitive ac transient excitation, trapping/de-trapping of electrons can follow much faster than trapping/de-trapping of holes so that a positive net charge occurs at internal grain boundaries oriented in parallel to the surface. As a result, photogenerated electrons are preferentially separated towards the bulk. As consequence, SPV signals are positive under ac modulated and repetitive ac transient excitation at the D2 transition.

4. Conclusions

Electronic transitions were studied in polycrystalline CVD diamond from near infrared to the deep UV by SPV techniques. A setup was developed for highly sensitive SPV measurements in the dc (Kelvin probe), ac (modulated) and ac (transient) regimes by using the same perforated electrode and charge amplifier. Numerous defect transitions were distinguished by SPV what was not possible, if regarding literature, by other methods before. Defect transitions were numbered by D1 to D8 with respect to the measurements in the dc (Kelvin probe) regime and appeared at 0.8–0.9, 1, 1.37, 1.78, 2.27, 3.15, 4.2 and 5.42 eV, respectively. In the ac (modulated) regime, several features were observed in the spectral range of transition D3 which gives a hint for even more transitions. Furthermore, transitions can be masked (or partially masked) by saturated signals in the ac (modulated) regime. Here, it will be helpful to extend the developed SPV set-up to measurements at high temperatures. SPV measurements in the ac (transients) regime showed the importance of disorder for relaxation of SPV signals excited in the D5 and D6 transitions at different photon energies. Phonon assisted transitions were detected at $E_g - E_x - h\nu_{LA,LO}$, $E_g - E_x + h\nu_{LA,LO}$ and $E_g - E_x + h\nu_{TO}$.

At present, a detailed analysis of SPV spectra and transients within a consistent model is not possible due to

the complexity of processes involved. For example, different and independent paths of charge transfer across crystallites and within grain boundaries shall be considered. In addition, measurement conditions influence the occupation of defect states. In next steps, measurement and preparation conditions will be varied in order to identify specific bulk and surface states.

It was shown that the developed SPV techniques are highly sensitive and well suitable for technology control of diamond as a semiconductor with an ultra-wide bandgap. We point out that the developed SPV techniques can be incorporated also for inline characterization if detecting, for example, signals only at dedicated photon energies. The developed methodology can become of great interest not only for research and development of diamond but also of other semiconductors with ultra-wide bandgap such as β -Ga₂O₃ (bandgap 4.8 eV [39]), AlN (bandgap 6.1 eV [40, 41]) or Al_xGa_{1-x}N (bandgap between 3.4 and 6.1 eV [42]).

Data availability statement

The data that support the findings of this study are available upon reasonable request from the authors.

Funding

This work was supported by the BMWi (ZIM-KK-5085302DF0 and ZIM-KK-5123601DF0).

Conflict of interest

The authors have no conflicts to disclose.

ORCID iDs

Thomas Dittrich  <https://orcid.org/0000-0002-2698-9481>
Steffen Fengler  <https://orcid.org/0000-0003-3999-7031>

References

- [1] Clark C D, Dean P J and Harris P V 1964 *Proc. R. Soc. A* **277** 312
- [2] Umezawa H 2018 *Mater. Sci. Semicond. Process.* **78** 147
- [3] Tordjman M 2022 *Nat. Electron.* **5** 21
- [4] Lu Y-J, Lin C-N and Shan C-X 2018 *Adv. Opt. Mater.* **6** 1800359
- [5] Nebel C E, Rezek B, Shin D, Uetsuka H and Yang N 2007 *J. Phys. D: Appl. Phys.* **40** 6443
- [6] Markham M L, Dodson J M, Scarsbrook G A, Twitchen D J, Balasubramanian G, Jelezko F and Wrachtrup J 2011 *Diam. Relat. Mater.* **20** 134
- [7] Heremans F J, Yale C G and Awschalom D D 2016 *Proc. IEEE* **104** 2009
- [8] Su L-X, Cao Y, Hao H-S, Zhao Q and Zhi J 2021 *Funct. Diam.* **1** 93
- [9] Zhang L, Zhu D, Nathanson G M and Hamers R J 2014 *Angew. Chem., Int. Ed.* **53** 9746
- [10] Knittel P *et al* 2020 *ChemCatChem* **12** 5548
- [11] Lu H-C, Lo J-I, Peng Y-C, Chou S-L, Cheng B-M and Chang H-C 2020 *ACS Appl. Mater. Interfaces* **12** 3847
- [12] Schreyvogel C, Polyakov V, Wunderlich R, Meijer J and Nebel C E 2015 *Sci. Rep.* **5** 12160
- [13] Kronik L and Shapira Y 1999 *Surf. Sci. Rep.* **37** 1
- [14] Dittrich T and Fengler S 2020 *Surface Photovoltage Analysis of Photoactive Materials* (Singapore: World Scientific)
- [15] Dittrich T, Fengler S and Nickel N 2021 *Phys. Status Solidi a* **218** 2100167
- [16] Monteiro O R 2019 *J. Mater. Sci.* **54** 2300
- [17] Zapol P, Sternberg M, Curtiss L A, Frauenheim T and Gruen D M 2001 *Phys. Rev. B* **65** 045403
- [18] Cleri F, Keblinski P, Colombo L, Wolf D and Phillpot S R 1999 *Europhys. Lett.* **46** 671
- [19] de Obaldia E I, Alcantar-Pena J J, Wittel F P, Veyan J F, Gallardo-Hernandez S, Koudriavtsev Y, Berman-Mendoza D and Auciallo O 2011 *Appl. Sci.* **11** 3990
- [20] Achatz P, Garrido J A, Stutzmann M, Williams O A, Gruen D M, Kromka A and Steinmüller D 2006 *Appl. Phys. Lett.* **88** 101908
- [21] Gajewski W, Achatz P, Williams O A, Haenen K, Bustarret E, Stutzmann M and Garrido J A 2009 *Phys. Rev. B* **79** 045206
- [22] Collins A T and Lightowlers E C 1968 *Phys. Rev.* **171** 843
- [23] Remes Z, Kromka A, Potmesil J and Vanecek M 2008 *Diam. Relat. Mater.* **17** 1311
- [24] Nebel C E 2003 *Semicond. Sci. Technol.* **18** S1
- [25] Rohrer E, Nebel C E, Stutzmann M, Flöter A, Zachai R, Jiang X and Klages C-P 1998 *Diam. Relat. Mater.* **7** 879
- [26] Nesládek M, Stals L M, Stesmans A, Iakubovskij K, Adriaenssens G J, Rosa J and Vanecek M 1998 *Appl. Phys. Lett.* **72** 3306
- [27] Rohrer E, Graeff C F O, Janssen R, Nebel C E, Stutzmann M, Güttler H and Zachai R 1996 *Phys. Rev. B* **54** 7874
- [28] Ristein J, Stein W and Ley L 1997 *Phys. Rev. Lett.* **78** 1803
- [29] Heremans F J, Fuchs G D, Wang C F, Hanson R and Awschalom D D 2009 *Appl. Phys. Lett.* **94** 152102
- [30] Dittrich T 2022 *AIP Adv.* **12** 065206
- [31] Stacey A *et al* 2019 *Adv. Mater. Interfaces* **6** 1801449
- [32] Challinger S, Baikie I, Birdwell A G and Strehle S 2017 *Phys. Status Solidi c* **14** 1700152
- [33] Challinger S, Baikie I and Birdwell A G 2017 *MRS Adv.* **2** 2229
- [34] Fengler S, Kriegel H, Schieda M, Gutzmann H, Klassen T, Wollgarten M and Dittrich T 2020 *ACS Appl. Mater. Interfaces* **12** 3140
- [35] Duzhko V, Timoshenko V Y, Koch F and Dittrich T 2001 *Phys. Rev. B* **64** 075204
- [36] Dittrich T, Bönisch S, Zabel P and Dube S 2008 *Rev. Sci. Instrum.* **79** 113903
- [37] Levine I, Hodes G, Snaith H J and Nayak P K 2017 *J. Phys. Chem. Lett.* **8** 2941
- [38] Simon P, Beck P, Rathi A, Stutzmann M and Garrido J A 2020 *Phys. Rev. B* **101** 205306
- [39] Xue H-W, He Q-M, Jian G-Z, Long S-B, Pang T and Liu M 2018 *Nanoscale Res. Lett.* **13** 290
- [40] Yamashita H, Fukui K, Misawa S and Yoshida S 1979 *J. Appl. Phys.* **50** 896
- [41] Guo Q, Nishio M, Ogawa H and Yoshida A 2001 *Phys. Rev. B* **64** 113105
- [42] Yoshida S, Misawa S and Gonda S 1982 *J. Appl. Phys.* **53** 6844